arXiv:1108.4569v1 [nucl-th] 23 Aug 2011

ECTP-2011-03

Fine-Grid Calculations for Stellar Electron and Positron Capture Rates on Fe-Isotopes

Jameel-Un Nabi*
Faculty of Engineering Sciences, GIK Institute of Engineering Sciences and Technology,
Topi 23640, Khyber Pakhtunkhwa, Pakistan and
Egyptian Center for Theoretical Physics (ECTP), MTI University, Al-Mokattam, Cairo, Egypt

Abdel Nasser Tawfik†
Egyptian Center for Theoretical Physics (ECTP), MTI University, Al-Mokattam, Cairo, Egypt

(Dated: August 24, 2011)

The acquisition of precise and reliable nuclear data is a prerequisite to success for stellar evolution and nucleosynthesis studies. Core-collapse simulators find it challenging to generate an explosion from the collapse of the core of massive stars. It is believed that a better understanding of the microphysics of core-collapse can lead to successful results. The weak interaction processes are able to trigger the collapse and control the lepton-to-baryon ratio (Y_e) of the core material. It is suggested that the temporal variation of Y_e within the core of a massive star has a pivotal role to play in the stellar evolution and a fine-tuning of this parameter at various stages of presupernova evolution is the key to generate an explosion. During the presupernova evolution of massive stars, isotopes of iron, mainly ^{54,55,56}Fe, are considered to be key players in controlling Y_e ratio via electron capture on these nuclide. Recently an improved microscopic calculation of weak interaction mediated rates for iron isotopes was introduced using the proton-neutron quasiparticle random phase approximation (pn-QRPA) theory. The pn-QRPA theory allows a microscopic *state-by-state* calculation of stellar capture rates which greatly increases the reliability of calculated rates. The results were suggestive of some fine-tuning of the Y_e ratio during various phases of stellar evolution. Here we present for the first time the fine-grid calculation of the electron and positron capture rates on ^{54,55,56}Fe. Core-collapse simulators may find this calculation suitable for interpolation purposes and for necessary incorporation in the stellar evolution codes.

PACS numbers: 21.60.Jz, 23.40.-s, 26.30.Jk, 26.50.+x, 97.10.Cv

I. INTRODUCTION

During the late phases of stellar evolution of massive stars, electron capture processes on heavy nuclei dominate the time evolution of the lepton-to-baryon ratio (Y_e) of the core material primarily due to the low entropy of the stellar core but also due to the resulting dominance of heavy nuclei over free nucleons [1]. Inside the iron core of massive stars, the electron capture occurs via the Gamow-Teller, GT$_+$, transitions changing protons in the $^1f_{7/2}$ level into neutrons in the $^1f_{5/2}$ levels. On the other hand the GT$_-$ strength is responsible for transforming a neutron into a proton (resulting in positron capture processes). It is conjectured that the electron captures on proton and positron captures on neutron play a very crucial role in the supernovae dynamics [2]. Due to the weak interaction processes, mainly electron and positron captures onto nuclei and $\beta^{\pm}$-decays of nuclei, the value of Y_e for a massive star changes from 1 (during hydrogen burning) to roughly 0.5 (at the beginning of carbon burning) and finally to around 0.42 just before the collapse leading to a supernova explosion [3]. The temporal variation of Y_e within the core of a massive star has a pivotal role to play in the stellar evolution and a fine-tuning of this parameter at various stages of presupernova evolution is the key to generate an explosion [4]. Furthermore, the electron capture rates is assumed to determine the mass of the core and thus the fate of the shock wave formed by the supernova explosion [4]. The calculation of electron and positron capture rates is very sensitive to the distribution of the GT$_{\pm}$ strength functions [5]. During the early phases of presupernova evolution, the electron chemical potential is of the same order of magnitude as the nuclear Q value and the capture rates are sensitive to the details of the GT$_{\pm}$ strength functions in daughter nuclei [6]. With proceeding collapse the stellar density

---

*Corresponding author; Electronic address: jameel@giki.edu.pk
†Electronic address: a.tawfik@eng.mti.edu.eg

increases by orders of magnitude and the resulting electron chemical potential is significantly higher than the nuclear Q value and then the capture rates are largely determined by the centroid and the total strength of the $\mathrm{GT}_{\pm}$ strength functions. A microscopic calculation of ground and excited state $\mathrm{GT}_{\pm}$ strength functions is the key to reliably estimate the stellar capture rate [6]. The positron captures are of great importance at high temperature and low density locations [7]. In such conditions, a rather high concentration of positron can be reached from $e^- + e^+ \leftrightarrow \gamma + \gamma$ equilibrium favoring the e^-e^+ pairs. The electron captures on proton and positron captures on neutron are considered important ingredients in the modeling of Type II supernovae [2].

The pn-QRPA theory [8] is an efficient way to microscopically generate $\mathrm{GT}_{\pm}$ strength functions which constitute a primary and nontrivial contribution to the weak interaction mediated rates among iron-regime nuclide. In this model a quasiparticle basis is first constructed with a pairing interaction. The random phase approximation (RPA) equation is then solved with a schematic GT residual interaction. The pn-QRPA model has been developed by Halbleib and Sorensen [8] by generalizing the usual RPA to describe charge-changing transitions of the type $(Z, N) \rightarrow (Z \pm 1, N \mp 1)$. The model is then extended to deformed nuclei (using Nilsson wave functions [9]) by Krumlinde and Möller [10]. Extension of the model to treat odd-odd nuclei and transitions from nuclear excited states has been done by Muto and collaborators [11]. The pn-QRPA is a simple and microscopic model. The pn-QRPA model has two big advantages for performing weak interaction calculations in stellar matter. Firstly it can handle any arbitrarily heavy system of nucleons since the calculation is performed in a luxurious model space of up to 7 major oscillator shells. The second advantage is even more important for the calculation of weak interaction rates in stellar environment. The prevailing temperature of the stellar matter is of the order of a few hundred kilo-electron volts to a few million-electron volts and $\mathrm{GT}_{\pm}$ transitions occur not only from nuclear ground state, but also from excited states. As experimental information about excited state strength functions seems inaccessible, Aufderheide [12] stressed much earlier the need to probe these strength functions theoretically. Today the pn-QRPA theory can be utilized to calculate $\mathrm{GT}_{\pm}$ strength distribution of *all* excited states of parent nucleus in a microscopic fashion and this feature of the pn-QRPA model greatly enhances the reliability of the calculated rates in stellar matter [13]. In other words, the pn-QRPA model seems to allow a microscopic state-by-state calculation of all stellar weak rates and the Brink hypothesis is not assumed in this model. Brink hypothesis [14] states that GT strength distribution on excited states is *identical* to that from ground state, shifted *only* by the excitation energy of the state. Recent calculations have pointed towards the fact that Brink hypothesis is not a safe approximation to use for calculation of stellar weak interaction rates [15–19].

Recently, weak interaction rates of isotopes of iron, ^{54,55,56}Fe, have been calculated using the pn-QRPA model [16]. There, the author reported that the calculated electron capture rates on these iron isotopes were overall in fair agreement with the large-scale shell model (LSSM) results [20]. However, it has been found that the calculated beta decay rates are suppressed by three to five orders of magnitude. In present paper, we present the fine-grid calculation of stellar electron and positron capture rates for iron-isotopes ^{54,55,56}Fe using pn-QRPA model. Recently, the improved pn-QRPA calculation has been introduced [16], where it was reported that the betterment resulted mainly from the incorporation of measured deformation values for these nuclei. A detailed analysis of the calculated ground and excited state $\mathrm{GT}_{\pm}$ strength distributions for ^{54,55,56}Fe and the capture rates has been presented in Ref. [21]. Due to the extreme conditions prevailing in the cores of massive stars, interpolation of calculated rates within large intervals of temperature-density points posed some uncertainty in the values of capture rates for collapse simulators [7]. As such the calculation is done on a detailed temperature and density grid pertinent to presupernova and supernova environment and should prove more suitable for running on simulation codes. In present work, a detailed calculation of electron and positron capture rates on ^{54,55,56}Fe is being presented for the first time at temperature-density intervals suitable for simulation purposes. Further, we also compare the pn-QRPA capture rates with previous key calculations for the astrophysically important range of stellar temperatures and densities. It is worthwhile to mention that the presence of ^{54,55,56}Fe in the stellar core is a result of the last phase of silicon burning.

The paper is organized as follows. Section II briefly discusses the formalism of the pn-QRPA calculations. In section III, the calculated results are present. Comparison with earlier calculations during presupernova evolution of massive stars is also included in this section. We summarize the main conclusions in Section IV. The fine-grid calculation of the stellar electron and positron capture rates on ^{54,55,56}Fe is presented in Table I.

II. NUCLEAR MODEL AND CALCULATION

The electron capture (ec) and positron capture (pc) rates of a transition from the i-th state of the parent to the j-th state of the daughter nucleus is given by

$$\lambda_{ij}^{ec(pc)} = \left[\frac{\ln 2}{D}\right] [f_{ij}(T, \rho, E_f)] \left[B(F)_{ij} + \left({g_A}/{g_V}\right)^2 B(GT)_{ij}\right]. \quad (1)$$

The value of D is reported in Ref. [22]. B_{ij} are the sum of reduced transition probabilities of the Fermi B(F) and GT transitions B(GT). Whereas for ^{54,56}Fe phonon transitions contribute, in the case of ^{55}Fe (odd-A case) two kinds of transitions are possible within the framework of the pn-QRPA model. One are the phonon transitions, where the odd quasiparticle acts as spectator and the other is the transitions of the odd quasiparticle itself. In the later case phonon correlations have been introduced to one-quasiparticle states in first-order perturbation [23]. The functions f_{ij} give the phase space integrals. Details of the calculations of phase space integrals and reduced transition probabilities in the pn-QRPA model can be found in Refs. [19, 21].

Therefore, the total electron (positron) capture rate per unit time per nucleus reads

$$\lambda^{ec(pc)} = \sum_{ij} P_i \lambda_{ij}^{ec(pc)}. \quad (2)$$

The summation over all initial and final states is to be carried out until satisfactory convergence in the rate calculations is achieved. Here P_i is the probability of occupation of parent excited states and follows the normal Boltzmann distribution. The pn-QRPA theory allows a microscopic state-by-state calculation of both sums present in Eq. (2). As discussed earlier in previous section, this feature of the pn-QRPA model greatly increases the reliability of the calculated rates in stellar matter where there exists a finite probability of occupation of excited states.

In order to further increase the reliability of the calculated capture rates experimental data were incorporated in the calculation wherever possible. In addition to the incorporation of the experimentally adopted value of the deformation parameter, the calculated excitation energies (along with their log ft values) were replaced with an experimental one when they were within 0.5 MeV of each other. The calculation presented in this work takes into consideration certain aspects. The missing measured states are inserted and inverse and mirror transitions are also taken into account. No theoretical levels have been replaced with the experimental ones beyond the excitation energy for which experimental compilations had no definite spin and/or parity. A state-by-state calculation of GT$_\pm$ strength has been performed for a total of 246 parent excited states in ^{54}Fe, 297 states for ^{55}Fe and 266 states for ^{56}Fe. For each parent excited state, transitions are calculated to 150 daughter excited states. The band widths of energy states are chosen according to the density of states to cover an excitation energy of $(15-20)$ MeV in parent and daughter nuclei. The summation in Eq. (2) has been done to ensure satisfactory convergence. The use of a separable interaction assisted in the incorporation of a luxurious model space of up to 7 major oscillator shells which in turn made possible to consider these many excited states both in parent and daughter nucleus.

Recently, the deformation parameter is being argued as an important parameter for QRPA calculations *at par* with the pairing parameter by Stetcu and Johnson [24]. As such rather than using deformations from some theoretical mass model (as used in earlier calculations of pn-QRPA rates e.g. [13, 25]), the experimentally adopted value of the deformation parameters for ^{54,56}Fe, extracted by relating the measured energy of the first 2^+ excited state with the quadrupole deformation, has been taken from Raman *et al.* [26]. For the case of ^{55}Fe, where such measurement apparently lacks, the deformation of the nucleus has been calculated as

$$\delta = \frac{125(Q_2)}{1.44(Z)(A)^{2/3}}, \quad (3)$$

where Z and A are the atomic and mass numbers, respectively. Q_2 is the electric quadrupole moment taken from Ref. [27]. Q-values are taken from the recent mass compilation of Audi *et al.* [28].

The incorporation of measured deformations for ^{54,56}Fe and a smart choice of strength parameters led to an improvement of the calculated GT$_\pm$ distributions compared to the measured ones [16]. In Table 1 of Ref. [16], it has been shown that the present pn-QRPA calculated GT$_\pm$ centroids and total $S_{\beta^\pm}$ strengths were in good agreement with available data for the even-even isotopes of iron. The table also shows marked improvement in the reported pn-QRPA calculation over the previous one [13].

The fine-grid calculation of stellar electron and positron capture rates on ^{54,55,56}Fe as a function of stellar temperature and density is given in Table I. The calculated rates are tabulated in logarithmic (to base 10) scale. It is simply a matter of convention to give -100 for instance to express that the rate is smaller than 10^{-100}. The first column gives $\log(\rho Y_e)$ in units of g cm^{-3}, where ρ is the baryon density and Y_e is the ratio of the electron number to the baryon number. Stellar temperatures (T_9) are given in 10^9 K. Stated also are the values of the Fermi energy of electrons in units of MeV. $\lambda^{ec}(\lambda^{pc})$ are the electron (positron) capture rates in units of sec^{-1}, Eq. (2). Core-collapse simulators may find it useful to employ the reported electron and positron capture rates on iron isotopes in their codes. The ASCII file of Table I is also available and can be received from the corresponding author upon request.

A detailed comparison of reported capture rates with previous calculations over a wide range of temperature and density has been presented earlier [21]. Here, we would like to present how the reported rates compare with previous calculations during temperature and density domains of astrophysical interest. For the sake of comparison, we took into consideration the pioneer calculations of FFN [7], those performed using the large-scale shell model (LSSM) [20] and the recently reported thermal QRPA (TQRPA) approach [29].

An analysis of the contribution of excited states to the total capture rates for these iron isotopes was performed earlier by Nabi [21]. There, it was shown that the electron capture rates have a significant contribution from parent excited states for the case of ^{54}Fe. The total capture rate is dominated by ground state contribution alone for the case of ^{55}Fe and the case of ^{56}Fe had a 50-50 contribution. Whenever ground state and low-lying states ($\sim$ 1 MeV) dominate the total capture rates the microscopic calculations of pn-QRPA and LSSM are found to be in very good agreement.

III. RESULTS AND COMPARISONS

Figure 1 depicts the comparison of electron capture rates on ^{54}Fe with LSSM and FFN calculations. The graph is drawn for temperature and density domain of astrophysical importance (oxygen shell burning and silicon core burning phases) for the case of ^{54}Fe. The upper panel displays the ratio of calculated rates to the LSSM rates, R_{ec}(QRPA/LSSM), while the lower panel shows a similar comparison with the FFN calculation, R_{ec}(QRPA/FFN). At lower stellar temperatures and densities the calculated electron capture rates are bigger than the corresponding LSSM rates by as much as a factor of four. The results agree at high temperatures and densities. During the early stages of the collapse the capture rates are very sensitive to the excited GT$_+$ strength distributions. It is reminded that LSSM approach allows for detailed nuclear spectroscopy but partially employs the Brink hypothesis. The pn-QRPA model, on the other hand, performs a microscopic calculation of all low-lying GT$_+$ strength distributions. At high densities the capture rates depend more on the centroid and total strength of the GT$_+$ functions. It was shown in Table 1 of Ref. [16] that the pn-QRPA calculated the centroid at a slightly higher energy in daughter ^{54}Mn nucleus as against LSSM centroid. But the effect was compensated by the calculation of a much higher total strength value as compared to LSSM strength. Accordingly the two results match well at high densities. The FFN electron capture rates are on the average bigger by an order of magnitude (lower panel of Figure 1) as compared to pn-QRPA rates. There are two main reasons for this enhancement in FFN rates. Firstly FFN did not take into consideration the quenching of the GT strength. FFN also did not take into effect the process of particle emission from excited states and accordingly their parent excitation energies extended well beyond the particle decay channel. For these reasons FFN rates were also bigger than LSSM rates by around an order of magnitude.

The electron capture rates on ^{55}Fe are argued to be most effective during the oxygen shell burning till around the ignition of the first stage of convective silicon shell burning of massive stars. Figure 2 depicts the comparison of the calculated electron capture rates on ^{55}Fe with LSSM (upper panel) and FFN (lower panel) calculations for the corresponding physical conditions. The upper panel shows a very good comparison of pn-QRPA and LSSM rates (within a factor of 2). Primarily the ground state but also a few low-lying excited GT$_+$ strength distributions play a key role in the calculation of total capture rates for this odd-A nucleus. LSSM performs a microscopic calculation of these low-lying strength functions (up to around 1 MeV). As mentioned earlier the ground state GT$_+$ strength function dominates the total capture rates on ^{55}Fe and the two calculations agree very well. The FFN rates are again bigger by an order of magnitude at high temperatures. The probability of occupation of high-lying excited states increases with stellar temperature and FFN rates are much bigger for reasons given above.

The comparison of electron capture rates on ^{56}Fe with previous calculations is shown in Figure 3. The capture rates on this isotope are very important for the pre-supernova phase of massive stars. As such Figure 3 shows the comparison up to $T_9[K] = 30$ and $\rho\, Y_e[g\, cm^{-3}] = 10^9$. Once again the comparison between pn-QRPA and LSSM is very good (for reasons mentioned earlier). FFN rates are again bigger for obvious reasons.

There are two key facts to keep in mind before we present a comparison of positron capture rates for ^{54,55,56}Fe. First, of all it is to be noted that positron capture rates are tens of orders of magnitude smaller than the corresponding electron capture rates. Secondly, these small numbers are fragile functions of the available phase space and can change appreciably by a mere change of 0.5 MeV in phase space calculations. The positron capture rates are more indicative of the uncertainties in calculation of the energy eigenvalues (for both parent and daughter states). Further it was shown in Ref. [21] that the ground state rate contributed at the maximum by only about 33% to the total positron capture rates. Figure 4 shows the comparison of the calculated positron capture rates on ^{54}Fe with the LSSM and FFN calculation for similar physical conditions as depicted in Figure 1. Here one sees that the pn-QRPA rates are suppressed by up to five orders of magnitude at low temperatures. The comparison improves as temperature increases. The comparison is similar in both upper and lower panels and does not change by increasing density by two orders of magnitude (from $\rho Y_e[gcm^{-3}] = 10^6$ to $\rho\, Y_e[g\, cm^{-3}] = 10^8$).

The comparison between pn-QRPA and LSSM improves for the case of ^{55}Fe (Figure 5) where the rates differ at the maximum by three orders of magnitude. The positron capture rates are in very good agreement with LSSM rates at high temperatures. Still better is the comparison case for ^{56}Fe (Figure 6). The FFN rates are bigger by up to four orders of magnitude.

Recently Dzhioev and collaborators [29] applied the pn-QRPA model extended to finite temperature by the thermofield dynamics formalism (referred to as TQRPA) and calculated electron capture rates on ^{54,56}Fe. It was reported by the authors that TQRPA and LSSM results matched well at low temperatures and high densities. At high temperatures the TQRPA rates were bigger than LSSM electron capture rates. Table II presents a mutual comparison between pn-QRPA, TQRPA and LSSM electron capture rates on these even-even isotopes of iron. It can be seen from Table II that TQRPA electron capture rates on ^{54}Fe are smaller by two (six) orders of magnitude at $T_9[K] = 1$ and $\rho\, Y_e[g\, cm^{-3}] = 10^7(10^8)$ as compared to pn-QRPA and LSSM rates. The comparison improves as temperature and density increase and TQRPA rates are doubled at $T_9[K] = 10$. As far as comparison of electron capture rates on ^{56}Fe is concerned, one again notes that TQRPA rates are smaller by up to seven orders of magnitude at low temperatures and densities. However by merely changing $T_9[K] = 1$ to $T_9[K] = 1.5$ the TQRPA rates gets up to 4 orders of magnitude bigger than the corresponding pn-QRPA and LSSM rates. It looks that TQRPA rates are very sensitive to temperature changes for the case of ^{56}Fe at low densities. The comparison improves with increasing stellar temperatures and densities. Once again at $T_9[K] = 10$ the TQRPA rates are roughly double the pn-QRPA and LSSM rates. Table II shows that the comparison between pn-QRPA and LSSM is comparatively far better and that TQRPA model requires further refinement.

IV. CONCLUSIONS

Precise and reliable nuclear data can lead to deciphering the elemental and isotopic abundances in Nature with more confidence and thereby derive meaningful constraints on the associated astrophysical models. The pn-QRPA model has a good track record of calculation of weak interaction rates both in terrestrial and stellar domains. The model has access to a huge model space making it possible to calculate weak rates for arbitrarily heavy system of nucleons. Further the model gets rid of the Brink hypothesis and calculates a *state-by-state* calculation of stellar capture rates which greatly increases the reliability of calculated rates. Incorporation of experimental deformation lead to a much improved version of this calculation. The model was used recently to calculate weak interaction mediated rates on iron isotopes, ^{54,55,56}Fe [16]. Electron capture on these isotopes of iron are mainly responsible for decreasing the electron-to-baryon ratio during the oxygen and silicon burning phases of massive stars. The corresponding positron capture rates are orders of magnitude smaller and accordingly less important for late stellar evolution of massive stars.

The calculated electron and positron capture rates are also compared against previous key calculations of weak rates. During the oxygen and silicon core burning phase of massive stars, the pn-QRPA electron capture rates on ^{54}Fe are around three times bigger than those calculated by LSSM. The comparison is very good for the case of ^{55,56}Fe. FFN electron capture rates are bigger by an order of magnitude. Orders of magnitude differences in electron capture rates exist between TQRPA and LSSM/pn-QRPA model.

The former calculations of positron capture rates on ^{54,55,56}Fe are 3-5 orders of magnitude bigger than the pn-QRPA rates. The LSSM positron capture rates on ^{56}Fe is in good agreement with reported rates.

The main idea of reporting this work is to present a fine-grid calculation of electron and positron capture rates on ^{54,55,56}Fe in stellar matter. Such tables (e.g. Table II of Ref. [30]) are of great utility for core-collapse simulators and also suitable for interpolation purposes. The fine-grid calculation is presented in Table I. The ASCII file of this table can also be requested from the author. Core-collapse simulators are encouraged to employ these rates in simulation codes to check for possible interesting outcomes.

Acknowledgment

J.-U. Nabi would like to acknowledge the support provided by TWAS and the local hospitality provided by the Egyptian Center for Theoretical Physics (ECTP), Cairo-Egypt, where this project was partially completed. J.-U. Nabi also wishes to acknowledge the support of research grant provided by the Higher Education Commission, Pakistan, through HEC Project No. 20-1283.

References

---

[1] H.A. Bethe, G. E. Brown, J. Applegate, and J. M. Lattimer, Nucl. Phys. **A324**, 487 (1979).
[2] J.-U. Nabi, Ph.D. Thesis, Heidelberg University Germany, 1999.
[3] D. Prialnik, *An Introduction to the theory of stellar structure and evolution* (Cambridge University Press, Cambridge, 2000).
[4] K. Kotake, K. Sato and K. Takahashi, Rep. Prog. Phys. **69**, 971 (2006).
[5] T. Rönnqvist et al., Nucl. Phys. **A563**, 225 (1993).
[6] M. B. Aufderheide, S. D. Bloom, G. J. Mathews and D. A. Resler, Phys. Rev. C **53**, 3139 (1996).
[7] G. M. Fuller, W. A. Fowler, M. J. Newman, Astrophys. J. Suppl. Ser **42**, 447 (1980); **48**, 279 (1982); Astrophys. J. **252**, 715 (1982); **293**, 1 (1985).
[8] J. A. Halbleib and R. A. Sorensen, Nucl. Phys. **A98**, 542 (1967).
[9] S. G. Nilsson, Mat. Fys. Medd. Dan. Vid. Selsk **29**, 16 (1955).
[10] J. Krumlinde and P. Möller P, Nucl. Phys. **A417**, 419 (1984).
[11] K. Muto, E. Bender, T. Oda and H. V. Klapdor, Z. Phys. A **341**, 407 (1992).
[12] M. B. Aufderheide, Nucl. Phys. **A526**, 161 (1991).
[13] J.-U. Nabi, H. V. Klapdor-Kleingrothaus, At. Data Nucl. Data Tables **88**, 237 (2004).
[14] D. M. Brink, Rep. Prog. Phys. **21**, 144 (1958).
[15] J.-U. Nabi, M. Sajjad, Phys. Rev. C **77**, 055802 (2008).
[16] J.-U. Nabi, Eur. Phys. J. **A40**, 223 (2009).
[17] J.-U. Nabi, Phys. Scripta **81**, 025901 (2010).
[18] J.-U. Nabi, Int. J. Mod. Phys. E **19**, 1 (2010).
[19] J.-U. Nabi, Adv. Sp. Res. **81**, 025901 (2010).
[20] K. Langanke and G. Martínez-Pinedo, Nucl. Phys. **A673**, 481 (2000).
[21] J.-U. Nabi, Astrophys. Space Sci. **331**, 537 (2011).
[22] G. P. Yost *et al.* (Particle Data Group), Phys. Lett. **B204**, 1 (1988).
[23] K. Muto, E. Bender, and H. V. Klapdor, Z. Phys. A **333**, 125 (1989).
[24] I. Stetcu and C. W. Johnson, Phys. Rev. C **69**, 024311 (2004).
[25] J.-U. Nabi, H. V. Klapdor-Kleingrothaus, At. Data Nucl. Data Tables **71**, 149 (1999).
[26] S. Raman, C. H. Malarkey, W. T. Milner, C. W. Nestor Jr and P. H. Stelson, At. Data Nucl. Data Tables **36**, 1 (1987).
[27] P. Möller and J. R. Nix, At. Data Nucl. Data Tables **26**, 165 (1981).
[28] G. Audi, A. H. Wapstra and C. Thibault C, Nucl. Phys. **A729**, 337 (2003).
[29] A. A. Dzhioev et al., Phys. Rev. C **81**, 015804 (2010).
[30] J.-U. Nabi, Phys. Rev. C **78**, 045801 (2008).

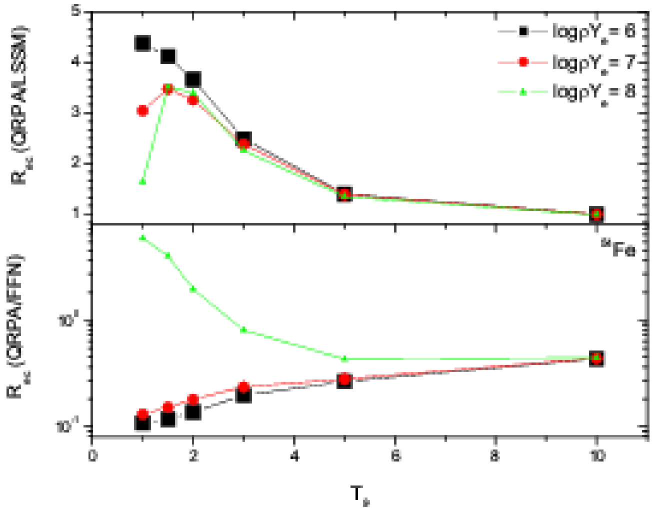

Fig. 1: (Color online) Ratios of reported electron capture rates to those calculated using LSSM [20] (upper panel) and by FFN [7] (lower panel) on ^{54}Fe as function of stellar temperatures and densities. T$_9$ gives the stellar temperature in units of 10^9 K. In the legend, $log\rho Y_e$ gives the log to base 10 of stellar density in units of gcm^{-3}.

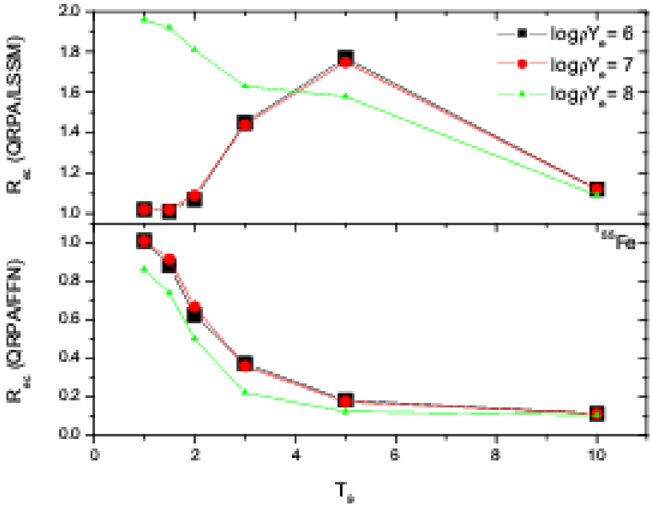

Fig. 2: (Color online) Same as figure 1 but for electron capture rates on ^{55}Fe.

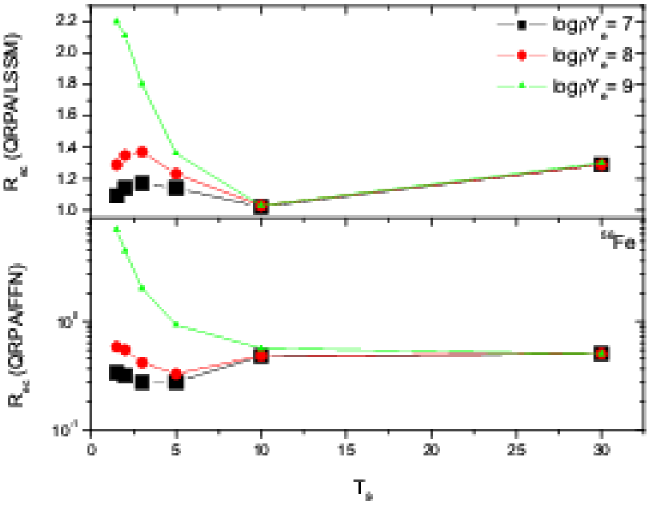

Fig. 3: (Color online) Same as figure 1 but for electron capture rates on ^{56}Fe.

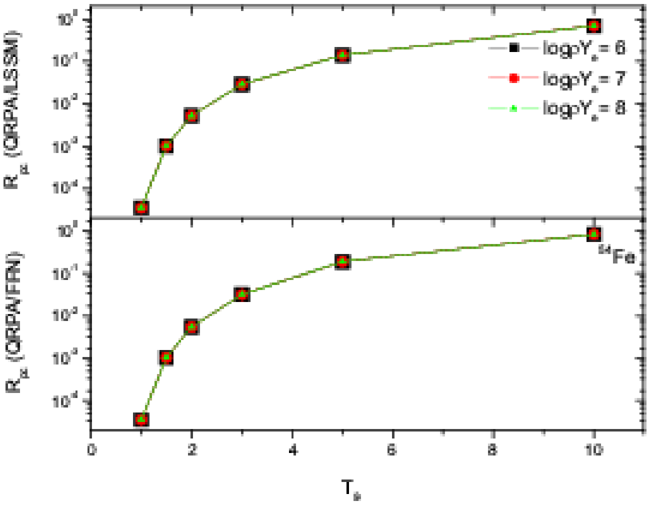

Fig. 4: (Color online) Same as figure 1 but for positron capture rates on ^{54}Fe.

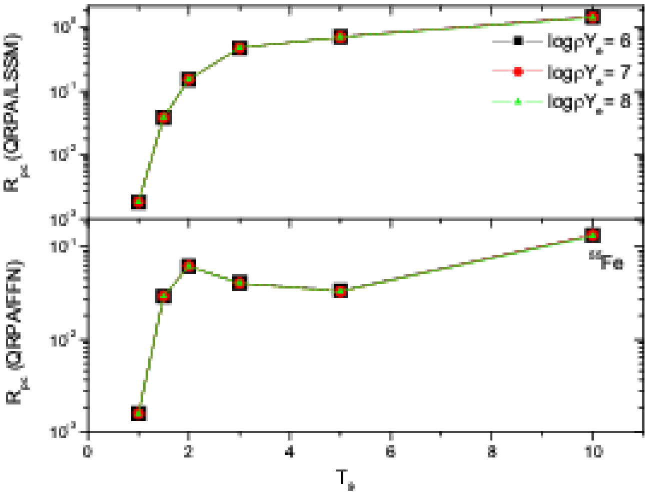

Fig. 5: (Color online) Same as figure 1 but for positron capture rates on ^{55}Fe.

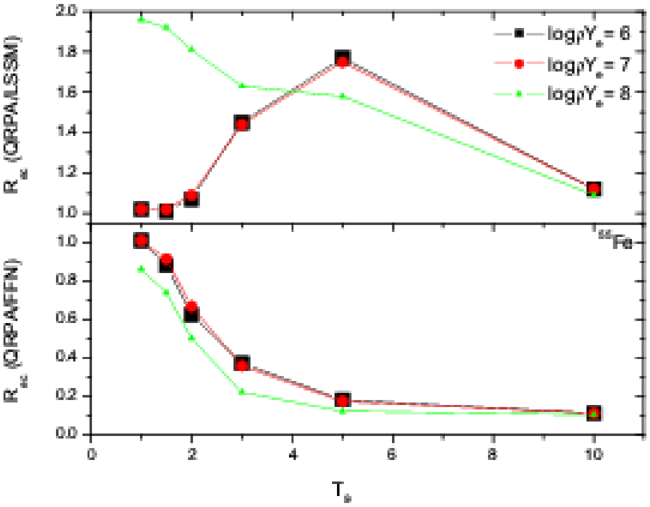

Fig. 6: (Color online) Same as figure 1 but for positron capture rates on ^{56}Fe.

Tab. I: Calculated electron and positron capture rates on ^{54,55,56}Fe on a fine-grid temperature-density scale. The calculated rates are tabulated in logarithmic (to base 10) scale. In the table, -100 means that the rate is smaller than 10^{-100}. For units see text.

$log\rho Y_e$	T_9	E_f	^{54}Fe		^{55}Fe		^{56}Fe	
			λ_{ec}	λ_{pc}	λ_{ec}	λ_{pc}	λ_{ec}	λ_{pc}
0.5	0.50	0.065	-24.273	-92.182	-11.945	-44.428	-47.582	-55.832
0.5	1.00	0.000	-14.748	-46.930	-9.415	-24.160	-25.753	-29.032
0.5	1.50	0.000	-11.123	-31.923	-8.077	-17.296	-17.897	-20.127
0.5	2.00	0.000	-9.119	-24.319	-7.159	-13.784	-13.821	-15.584
0.5	2.50	0.000	-7.758	-19.668	-6.382	-11.623	-11.293	-12.799
0.5	3.00	0.000	-6.738	-16.496	-5.716	-10.136	-9.554	-10.895
0.5	3.50	0.000	-5.935	-14.178	-5.155	-9.027	-8.273	-9.494
0.5	4.00	0.000	-5.280	-12.402	-4.680	-8.146	-7.282	-8.407
0.5	4.50	0.000	-4.734	-10.992	-4.273	-7.413	-6.487	-7.529
0.5	5.00	0.000	-4.268	-9.842	-3.917	-6.784	-5.831	-6.798
0.5	5.50	0.000	-3.864	-8.885	-3.603	-6.234	-5.277	-6.176
0.5	6.00	0.000	-3.508	-8.072	-3.322	-5.746	-4.800	-5.638
0.5	6.50	0.000	-3.191	-7.372	-3.068	-5.310	-4.383	-5.165
0.5	7.00	0.000	-2.904	-6.762	-2.835	-4.916	-4.013	-4.745
0.5	7.50	0.000	-2.644	-6.224	-2.620	-4.558	-3.682	-4.369
0.5	8.00	0.000	-2.405	-5.745	-2.419	-4.229	-3.382	-4.028
0.5	8.50	0.000	-2.185	-5.315	-2.230	-3.926	-3.108	-3.718
0.5	9.00	0.000	-1.980	-4.926	-2.052	-3.645	-2.856	-3.433
0.5	9.50	0.000	-1.788	-4.572	-1.882	-3.383	-2.623	-3.171
0.5	10.00	0.000	-1.609	-4.248	-1.719	-3.138	-2.406	-2.927
0.5	15.00	0.000	-0.264	-2.032	-0.389	-1.322	-0.809	-1.173
0.5	20.00	0.000	0.601	-0.757	0.555	-0.187	0.203	-0.093
0.5	25.00	0.000	1.220	0.112	1.245	0.600	0.915	0.661
0.5	30.00	0.000	1.699	0.762	1.770	1.187	1.453	1.233
1.0	0.50	0.113	-23.793	-92.662	-11.464	-44.909	-47.102	-56.312
1.0	1.00	0.000	-14.747	-46.931	-9.413	-24.161	-25.752	-29.033
1.0	1.50	0.000	-11.122	-31.923	-8.077	-17.296	-17.897	-20.127
1.0	2.00	0.000	-9.119	-24.319	-7.159	-13.784	-13.820	-15.584
1.0	2.50	0.000	-7.758	-19.668	-6.381	-11.623	-11.292	-12.799
1.0	3.00	0.000	-6.738	-16.496	-5.716	-10.136	-9.553	-10.895
1.0	3.50	0.000	-5.934	-14.178	-5.155	-9.027	-8.272	-9.494
1.0	4.00	0.000	-5.280	-12.401	-4.680	-8.145	-7.282	-8.407
1.0	4.50	0.000	-4.733	-10.992	-4.272	-7.412	-6.487	-7.528
1.0	5.00	0.000	-4.268	-9.842	-3.917	-6.783	-5.831	-6.798
1.0	5.50	0.000	-3.863	-8.884	-3.603	-6.233	-5.277	-6.176
1.0	6.00	0.000	-3.508	-8.072	-3.322	-5.746	-4.800	-5.637
1.0	6.50	0.000	-3.190	-7.372	-3.068	-5.310	-4.382	-5.165
1.0	7.00	0.000	-2.904	-6.762	-2.835	-4.916	-4.013	-4.745
1.0	7.50	0.000	-2.644	-6.223	-2.619	-4.557	-3.681	-4.368
1.0	8.00	0.000	-2.405	-5.744	-2.418	-4.229	-3.381	-4.028
1.0	8.50	0.000	-2.184	-5.314	-2.230	-3.925	-3.107	-3.717
1.0	9.00	0.000	-1.979	-4.925	-2.051	-3.644	-2.856	-3.433
1.0	9.50	0.000	-1.788	-4.571	-1.881	-3.382	-2.622	-3.170
1.0	10.00	0.000	-1.608	-4.247	-1.719	-3.137	-2.405	-2.927
1.0	15.00	0.000	-0.263	-2.031	-0.388	-1.322	-0.808	-1.172
1.0	20.00	0.000	0.602	-0.756	0.556	-0.186	0.204	-0.092
1.0	25.00	0.000	1.221	0.113	1.246	0.601	0.916	0.662
1.0	30.00	0.000	1.700	0.763	1.771	1.188	1.454	1.234

$log\rho Y_e$	T_9	E_f	^{54}Fe		^{55}Fe		^{56}Fe	
			λ_{ec}	λ_{pc}	λ_{ec}	λ_{pc}	λ_{ec}	λ_{pc}
1.5	0.50	0.162	-23.295	-93.160	-10.966	-45.406	-46.604	-56.810
1.5	1.00	0.002	-14.741	-46.936	-9.408	-24.166	-25.746	-29.038
1.5	1.50	0.000	-11.122	-31.923	-8.077	-17.297	-17.896	-20.128
1.5	2.00	0.000	-9.119	-24.319	-7.159	-13.784	-13.820	-15.584
1.5	2.50	0.000	-7.758	-19.668	-6.381	-11.623	-11.292	-12.799
1.5	3.00	0.000	-6.738	-16.496	-5.716	-10.136	-9.553	-10.895
1.5	3.50	0.000	-5.934	-14.178	-5.155	-9.026	-8.272	-9.494
1.5	4.00	0.000	-5.280	-12.401	-4.680	-8.145	-7.282	-8.407
1.5	4.50	0.000	-4.733	-10.991	-4.272	-7.412	-6.487	-7.528
1.5	5.00	0.000	-4.268	-9.842	-3.917	-6.783	-5.831	-6.798
1.5	5.50	0.000	-3.863	-8.884	-3.603	-6.233	-5.277	-6.176
1.5	6.00	0.000	-3.507	-8.072	-3.322	-5.746	-4.800	-5.637
1.5	6.50	0.000	-3.190	-7.372	-3.067	-5.310	-4.382	-5.164
1.5	7.00	0.000	-2.904	-6.761	-2.834	-4.916	-4.013	-4.745
1.5	7.50	0.000	-2.643	-6.223	-2.619	-4.557	-3.681	-4.368
1.5	8.00	0.000	-2.404	-5.744	-2.418	-4.228	-3.381	-4.028
1.5	8.50	0.000	-2.184	-5.314	-2.229	-3.925	-3.107	-3.717
1.5	9.00	0.000	-1.979	-4.925	-2.051	-3.644	-2.855	-3.433
1.5	9.50	0.000	-1.788	-4.571	-1.881	-3.382	-2.622	-3.170
1.5	10.00	0.000	-1.608	-4.247	-1.719	-3.137	-2.405	-2.927
1.5	15.00	0.000	-0.263	-2.031	-0.388	-1.321	-0.808	-1.171
1.5	20.00	0.000	0.602	-0.755	0.557	-0.185	0.204	-0.092
1.5	25.00	0.000	1.221	0.113	1.246	0.602	0.916	0.662
1.5	30.00	0.000	1.700	0.764	1.771	1.188	1.454	1.234
2.0	0.50	0.212	-22.795	-93.660	-10.466	-45.906	-46.104	-57.310
2.0	1.00	0.005	-14.725	-46.953	-9.392	-24.183	-25.730	-29.055
2.0	1.50	0.000	-11.121	-31.925	-8.075	-17.298	-17.895	-20.129
2.0	2.00	0.000	-9.118	-24.319	-7.158	-13.784	-13.820	-15.584
2.0	2.50	0.000	-7.758	-19.668	-6.381	-11.623	-11.292	-12.799
2.0	3.00	0.000	-6.738	-16.496	-5.716	-10.136	-9.553	-10.895
2.0	3.50	0.000	-5.934	-14.178	-5.155	-9.026	-8.272	-9.494
2.0	4.00	0.000	-5.280	-12.401	-4.680	-8.145	-7.282	-8.407
2.0	4.50	0.000	-4.733	-10.991	-4.272	-7.412	-6.487	-7.528
2.0	5.00	0.000	-4.267	-9.842	-3.917	-6.783	-5.831	-6.797
2.0	5.50	0.000	-3.863	-8.884	-3.603	-6.233	-5.277	-6.176
2.0	6.00	0.000	-3.507	-8.072	-3.322	-5.746	-4.799	-5.637
2.0	6.50	0.000	-3.190	-7.372	-3.067	-5.310	-4.382	-5.164
2.0	7.00	0.000	-2.904	-6.761	-2.834	-4.916	-4.013	-4.745
2.0	7.50	0.000	-2.643	-6.223	-2.619	-4.557	-3.681	-4.368
2.0	8.00	0.000	-2.404	-5.744	-2.418	-4.228	-3.381	-4.028
2.0	8.50	0.000	-2.184	-5.314	-2.229	-3.925	-3.107	-3.717
2.0	9.00	0.000	-1.979	-4.925	-2.051	-3.644	-2.855	-3.433
2.0	9.50	0.000	-1.788	-4.571	-1.881	-3.382	-2.622	-3.170
2.0	10.00	0.000	-1.608	-4.247	-1.719	-3.137	-2.405	-2.927
2.0	15.00	0.000	-0.263	-2.031	-0.388	-1.321	-0.808	-1.171
2.0	20.00	0.000	0.602	-0.755	0.557	-0.185	0.204	-0.092
2.0	25.00	0.000	1.221	0.113	1.246	0.602	0.916	0.662
2.0	30.00	0.000	1.700	0.764	1.772	1.189	1.454	1.235

$log\rho Y_e$	T_9	E_f	^{54}Fe		^{55}Fe		^{56}Fe	
			λ_{ec}	λ_{pc}	λ_{ec}	λ_{pc}	λ_{ec}	λ_{pc}
2.5	0.50	0.261	-22.295	-94.160	-9.966	-46.407	-45.604	-57.810
2.5	1.00	0.015	-14.673	-47.005	-9.340	-24.235	-25.678	-29.106
2.5	1.50	0.002	-11.117	-31.928	-8.072	-17.301	-17.892	-20.132
2.5	2.00	0.000	-9.118	-24.320	-7.158	-13.785	-13.819	-15.585
2.5	2.50	0.000	-7.758	-19.668	-6.381	-11.623	-11.292	-12.799
2.5	3.00	0.000	-6.738	-16.496	-5.716	-10.136	-9.553	-10.895
2.5	3.50	0.000	-5.934	-14.178	-5.155	-9.026	-8.272	-9.494
2.5	4.00	0.000	-5.280	-12.401	-4.680	-8.145	-7.281	-8.407
2.5	4.50	0.000	-4.733	-10.991	-4.272	-7.412	-6.487	-7.528
2.5	5.00	0.000	-4.267	-9.842	-3.917	-6.783	-5.831	-6.797
2.5	5.50	0.000	-3.863	-8.884	-3.603	-6.233	-5.276	-6.176
2.5	6.00	0.000	-3.507	-8.071	-3.322	-5.746	-4.799	-5.637
2.5	6.50	0.000	-3.190	-7.372	-3.067	-5.310	-4.382	-5.164
2.5	7.00	0.000	-2.904	-6.761	-2.834	-4.916	-4.013	-4.745
2.5	7.50	0.000	-2.643	-6.223	-2.619	-4.557	-3.681	-4.368
2.5	8.00	0.000	-2.404	-5.744	-2.418	-4.228	-3.381	-4.028
2.5	8.50	0.000	-2.184	-5.314	-2.229	-3.925	-3.107	-3.717
2.5	9.00	0.000	-1.979	-4.925	-2.051	-3.644	-2.855	-3.433
2.5	9.50	0.000	-1.787	-4.571	-1.881	-3.382	-2.622	-3.170
2.5	10.00	0.000	-1.608	-4.247	-1.718	-3.137	-2.405	-2.927
2.5	15.00	0.000	-0.263	-2.031	-0.388	-1.321	-0.808	-1.171
2.5	20.00	0.000	0.602	-0.755	0.557	-0.185	0.205	-0.092
2.5	25.00	0.000	1.221	0.114	1.246	0.602	0.916	0.662
2.5	30.00	0.000	1.700	0.764	1.772	1.189	1.454	1.235
3.0	0.50	0.311	-21.795	-94.661	-9.466	-46.908	-45.103	-58.311
3.0	1.00	0.046	-14.519	-47.159	-9.186	-24.389	-25.524	-29.261
3.0	1.50	0.005	-11.106	-31.939	-8.061	-17.312	-17.881	-20.143
3.0	2.00	0.001	-9.115	-24.322	-7.155	-13.787	-13.817	-15.588
3.0	2.50	0.001	-7.757	-19.669	-6.380	-11.624	-11.291	-12.800
3.0	3.00	0.000	-6.737	-16.497	-5.716	-10.136	-9.553	-10.895
3.0	3.50	0.000	-5.934	-14.178	-5.155	-9.027	-8.272	-9.494
3.0	4.00	0.000	-5.280	-12.401	-4.680	-8.145	-7.281	-8.407
3.0	4.50	0.000	-4.733	-10.992	-4.272	-7.412	-6.487	-7.528
3.0	5.00	0.000	-4.267	-9.842	-3.917	-6.783	-5.831	-6.798
3.0	5.50	0.000	-3.863	-8.884	-3.603	-6.233	-5.276	-6.176
3.0	6.00	0.000	-3.507	-8.072	-3.322	-5.746	-4.799	-5.637
3.0	6.50	0.000	-3.190	-7.372	-3.067	-5.310	-4.382	-5.164
3.0	7.00	0.000	-2.904	-6.761	-2.834	-4.916	-4.013	-4.745
3.0	7.50	0.000	-2.643	-6.223	-2.619	-4.557	-3.681	-4.368
3.0	8.00	0.000	-2.404	-5.744	-2.418	-4.228	-3.381	-4.028
3.0	8.50	0.000	-2.184	-5.314	-2.229	-3.925	-3.107	-3.717
3.0	9.00	0.000	-1.979	-4.925	-2.051	-3.644	-2.855	-3.433
3.0	9.50	0.000	-1.787	-4.571	-1.881	-3.382	-2.622	-3.170
3.0	10.00	0.000	-1.608	-4.247	-1.718	-3.137	-2.405	-2.927
3.0	15.00	0.000	-0.263	-2.031	-0.388	-1.321	-0.808	-1.171
3.0	20.00	0.000	0.602	-0.755	0.557	-0.185	0.205	-0.092
3.0	25.00	0.000	1.221	0.114	1.246	0.602	0.916	0.662
3.0	30.00	0.000	1.700	0.764	1.772	1.189	1.454	1.235

$log\rho Y_e$	T_9	E_f	^{54}Fe		^{55}Fe		^{56}Fe	
			λ_{ec}	λ_{pc}	λ_{ec}	λ_{pc}	λ_{ec}	λ_{pc}
3.5	0.50	0.361	-21.296	-95.164	-8.967	-47.411	-44.600	-58.814
3.5	1.00	0.115	-14.172	-47.507	-8.839	-24.737	-25.176	-29.608
3.5	1.50	0.015	-11.072	-31.974	-8.026	-17.347	-17.846	-20.178
3.5	2.00	0.004	-9.108	-24.330	-7.148	-13.795	-13.809	-15.595
3.5	2.50	0.002	-7.754	-19.672	-6.377	-11.627	-11.288	-12.803
3.5	3.00	0.001	-6.736	-16.498	-5.714	-10.138	-9.551	-10.897
3.5	3.50	0.001	-5.933	-14.179	-5.154	-9.027	-8.271	-9.495
3.5	4.00	0.001	-5.279	-12.402	-4.679	-8.146	-7.281	-8.407
3.5	4.50	0.000	-4.733	-10.992	-4.272	-7.412	-6.486	-7.529
3.5	5.00	0.000	-4.267	-9.842	-3.916	-6.783	-5.830	-6.798
3.5	5.50	0.000	-3.863	-8.884	-3.603	-6.233	-5.276	-6.176
3.5	6.00	0.000	-3.507	-8.072	-3.322	-5.746	-4.799	-5.637
3.5	6.50	0.000	-3.190	-7.372	-3.067	-5.310	-4.382	-5.164
3.5	7.00	0.000	-2.904	-6.761	-2.834	-4.916	-4.012	-4.745
3.5	7.50	0.000	-2.643	-6.223	-2.619	-4.557	-3.681	-4.368
3.5	8.00	0.000	-2.404	-5.744	-2.418	-4.228	-3.381	-4.028
3.5	8.50	0.000	-2.184	-5.314	-2.229	-3.925	-3.107	-3.717
3.5	9.00	0.000	-1.979	-4.925	-2.051	-3.644	-2.855	-3.433
3.5	9.50	0.000	-1.787	-4.571	-1.881	-3.382	-2.622	-3.170
3.5	10.00	0.000	-1.608	-4.247	-1.718	-3.137	-2.405	-2.927
3.5	15.00	0.000	-0.263	-2.031	-0.388	-1.321	-0.808	-1.171
3.5	20.00	0.000	0.602	-0.755	0.557	-0.185	0.205	-0.092
3.5	25.00	0.000	1.221	0.114	1.246	0.602	0.916	0.662
3.5	30.00	0.000	1.700	0.764	1.772	1.189	1.454	1.235
4.0	0.50	0.411	-20.798	-95.673	-8.467	-47.920	-44.090	-59.323
4.0	1.00	0.209	-13.700	-47.981	-8.366	-25.211	-24.702	-30.083
4.0	1.50	0.047	-10.965	-32.081	-7.920	-17.454	-17.739	-20.285
4.0	2.00	0.014	-9.084	-24.354	-7.124	-13.819	-13.785	-15.619
4.0	2.50	0.006	-7.746	-19.681	-6.369	-11.635	-11.280	-12.811
4.0	3.00	0.004	-6.732	-16.502	-5.710	-10.142	-9.547	-10.901
4.0	3.50	0.002	-5.931	-14.181	-5.152	-9.030	-8.269	-9.497
4.0	4.00	0.002	-5.278	-12.403	-4.678	-8.147	-7.280	-8.409
4.0	4.50	0.001	-4.732	-10.993	-4.271	-7.413	-6.485	-7.530
4.0	5.00	0.001	-4.267	-9.843	-3.916	-6.784	-5.830	-6.798
4.0	5.50	0.001	-3.863	-8.885	-3.602	-6.234	-5.276	-6.176
4.0	6.00	0.001	-3.507	-8.072	-3.321	-5.746	-4.799	-5.638
4.0	6.50	0.001	-3.190	-7.372	-3.067	-5.310	-4.382	-5.165
4.0	7.00	0.000	-2.903	-6.762	-2.834	-4.916	-4.012	-4.745
4.0	7.50	0.000	-2.643	-6.223	-2.619	-4.557	-3.681	-4.368
4.0	8.00	0.000	-2.404	-5.744	-2.418	-4.228	-3.381	-4.028
4.0	8.50	0.000	-2.184	-5.314	-2.229	-3.925	-3.107	-3.717
4.0	9.00	0.000	-1.979	-4.925	-2.051	-3.644	-2.855	-3.433
4.0	9.50	0.000	-1.787	-4.571	-1.881	-3.382	-2.622	-3.170
4.0	10.00	0.000	-1.608	-4.247	-1.718	-3.137	-2.405	-2.927
4.0	15.00	0.000	-0.263	-2.031	-0.388	-1.321	-0.808	-1.171
4.0	20.00	0.000	0.602	-0.755	0.557	-0.185	0.205	-0.092
4.0	25.00	0.000	1.221	0.114	1.246	0.602	0.916	0.662
4.0	30.00	0.000	1.700	0.764	1.772	1.189	1.454	1.235

$log\rho Y_e$	T_9	E_f	^{54}Fe		^{55}Fe		^{56}Fe	
			λ_{ec}	λ_{pc}	λ_{ec}	λ_{pc}	λ_{ec}	λ_{pc}
4.5	0.50	0.464	-20.304	-96.203	-7.969	-48.449	-43.561	-59.852
4.5	1.00	0.309	-13.203	-48.487	-7.867	-25.717	-24.196	-30.588
4.5	1.50	0.130	-10.690	-32.359	-7.644	-17.732	-17.461	-20.563
4.5	2.00	0.044	-9.010	-24.429	-7.050	-13.894	-13.710	-15.694
4.5	2.50	0.020	-7.718	-19.708	-6.342	-11.663	-11.252	-12.839
4.5	3.00	0.011	-6.719	-16.515	-5.698	-10.154	-9.534	-10.914
4.5	3.50	0.007	-5.924	-14.188	-5.145	-9.037	-8.262	-9.504
4.5	4.00	0.005	-5.273	-12.408	-4.674	-8.152	-7.275	-8.413
4.5	4.50	0.004	-4.729	-10.996	-4.268	-7.416	-6.483	-7.532
4.5	5.00	0.003	-4.265	-9.845	-3.914	-6.786	-5.828	-6.800
4.5	5.50	0.002	-3.861	-8.886	-3.601	-6.235	-5.274	-6.178
4.5	6.00	0.002	-3.506	-8.073	-3.320	-5.747	-4.798	-5.639
4.5	6.50	0.002	-3.189	-7.373	-3.066	-5.311	-4.381	-5.166
4.5	7.00	0.001	-2.903	-6.762	-2.833	-4.916	-4.012	-4.745
4.5	7.50	0.001	-2.643	-6.224	-2.618	-4.558	-3.680	-4.369
4.5	8.00	0.001	-2.404	-5.745	-2.417	-4.229	-3.380	-4.028
4.5	8.50	0.001	-2.183	-5.314	-2.229	-3.926	-3.107	-3.718
4.5	9.00	0.001	-1.978	-4.925	-2.050	-3.644	-2.855	-3.433
4.5	9.50	0.001	-1.787	-4.571	-1.880	-3.382	-2.622	-3.170
4.5	10.00	0.001	-1.608	-4.247	-1.718	-3.137	-2.405	-2.927
4.5	15.00	0.000	-0.263	-2.031	-0.388	-1.321	-0.807	-1.171
4.5	20.00	0.000	0.602	-0.755	0.557	-0.185	0.205	-0.092
4.5	25.00	0.000	1.222	0.114	1.246	0.602	0.916	0.662
4.5	30.00	0.000	1.700	0.764	1.772	1.189	1.454	1.235
5.0	0.50	0.522	-19.818	-96.792	-7.471	-49.038	-42.972	-60.441
5.0	1.00	0.413	-12.703	-49.013	-7.362	-26.243	-23.670	-31.115
5.0	1.50	0.265	-10.243	-32.814	-7.195	-18.188	-17.005	-21.019
5.0	2.00	0.128	-8.799	-24.643	-6.839	-14.108	-13.497	-15.908
5.0	2.50	0.062	-7.634	-19.793	-6.258	-11.748	-11.167	-12.924
5.0	3.00	0.035	-6.679	-16.556	-5.658	-10.195	-9.494	-10.954
5.0	3.50	0.023	-5.902	-14.211	-5.123	-9.059	-8.239	-9.527
5.0	4.00	0.016	-5.260	-12.421	-4.660	-8.165	-7.261	-8.427
5.0	4.50	0.012	-4.720	-11.005	-4.259	-7.425	-6.473	-7.542
5.0	5.00	0.009	-4.258	-9.851	-3.908	-6.792	-5.821	-6.807
5.0	5.50	0.007	-3.857	-8.891	-3.596	-6.240	-5.270	-6.182
5.0	6.00	0.006	-3.502	-8.076	-3.317	-5.751	-4.794	-5.642
5.0	6.50	0.005	-3.186	-7.376	-3.064	-5.313	-4.378	-5.168
5.0	7.00	0.004	-2.901	-6.764	-2.831	-4.919	-4.009	-4.748
5.0	7.50	0.004	-2.641	-6.226	-2.617	-4.559	-3.679	-4.370
5.0	8.00	0.003	-2.402	-5.746	-2.416	-4.230	-3.379	-4.029
5.0	8.50	0.003	-2.182	-5.315	-2.228	-3.927	-3.106	-3.719
5.0	9.00	0.002	-1.977	-4.926	-2.049	-3.645	-2.854	-3.434
5.0	9.50	0.002	-1.786	-4.572	-1.880	-3.383	-2.621	-3.171
5.0	10.00	0.002	-1.607	-4.248	-1.717	-3.138	-2.404	-2.927
5.0	15.00	0.001	-0.263	-2.031	-0.388	-1.321	-0.807	-1.172
5.0	20.00	0.000	0.602	-0.755	0.557	-0.185	0.205	-0.092
5.0	25.00	0.000	1.222	0.114	1.246	0.602	0.916	0.662
5.0	30.00	0.000	1.700	0.764	1.772	1.189	1.454	1.235

$log\rho Y_e$	T_9	E_f	^{54}Fe		^{55}Fe		^{56}Fe	
			λ_{ec}	λ_{pc}	λ_{ec}	λ_{pc}	λ_{ec}	λ_{pc}
5.5	0.50	0.598	-19.338	-97.550	-6.959	-49.797	-42.214	-61.200
5.5	1.00	0.528	-12.201	-49.592	-6.844	-26.822	-23.091	-31.694
5.5	1.50	0.423	-9.742	-33.344	-6.689	-18.718	-16.475	-21.549
5.5	2.00	0.295	-8.389	-25.063	-6.430	-14.528	-13.076	-16.329
5.5	2.50	0.180	-7.400	-20.031	-6.026	-11.986	-10.929	-13.162
5.5	3.00	0.110	-6.556	-16.680	-5.536	-10.320	-9.369	-11.079
5.5	3.50	0.072	-5.832	-14.281	-5.054	-9.129	-8.169	-9.597
5.5	4.00	0.050	-5.217	-12.465	-4.618	-8.209	-7.218	-8.470
5.5	4.50	0.038	-4.692	-11.033	-4.231	-7.454	-6.445	-7.570
5.5	5.00	0.029	-4.238	-9.871	-3.888	-6.812	-5.801	-6.827
5.5	5.50	0.023	-3.842	-8.905	-3.582	-6.254	-5.255	-6.197
5.5	6.00	0.019	-3.492	-8.087	-3.306	-5.762	-4.784	-5.653
5.5	6.50	0.016	-3.178	-7.384	-3.055	-5.322	-4.370	-5.177
5.5	7.00	0.013	-2.894	-6.771	-2.825	-4.925	-4.003	-4.754
5.5	7.50	0.012	-2.636	-6.231	-2.611	-4.565	-3.673	-4.376
5.5	8.00	0.010	-2.398	-5.750	-2.412	-4.235	-3.375	-4.034
5.5	8.50	0.009	-2.179	-5.319	-2.224	-3.930	-3.102	-3.722
5.5	9.00	0.008	-1.974	-4.929	-2.046	-3.648	-2.851	-3.437
5.5	9.50	0.007	-1.784	-4.574	-1.877	-3.385	-2.618	-3.174
5.5	10.00	0.006	-1.605	-4.250	-1.715	-3.140	-2.402	-2.930
5.5	15.00	0.003	-0.262	-2.032	-0.387	-1.322	-0.807	-1.172
5.5	20.00	0.001	0.602	-0.755	0.557	-0.185	0.205	-0.092
5.5	25.00	0.001	1.222	0.113	1.246	0.602	0.916	0.662
5.5	30.00	0.001	1.700	0.764	1.772	1.189	1.454	1.235
6.0	0.50	0.713	-18.832	-98.714	-6.389	-50.961	-41.050	-62.364
6.0	1.00	0.672	-11.680	-50.316	-6.287	-27.546	-22.367	-32.418
6.0	1.50	0.604	-9.216	-33.952	-6.150	-19.325	-15.868	-22.156
6.0	2.00	0.512	-7.876	-25.610	-5.919	-15.075	-12.529	-16.875
6.0	2.50	0.405	-6.961	-20.484	-5.595	-12.439	-10.476	-13.614
6.0	3.00	0.299	-6.244	-16.998	-5.230	-10.637	-9.051	-11.397
6.0	3.50	0.214	-5.630	-14.486	-4.856	-9.334	-7.964	-9.802
6.0	4.00	0.156	-5.086	-12.598	-4.489	-8.341	-7.085	-8.603
6.0	4.50	0.117	-4.603	-11.123	-4.144	-7.543	-6.355	-7.659
6.0	5.00	0.091	-4.176	-9.934	-3.827	-6.875	-5.739	-6.889
6.0	5.50	0.073	-3.797	-8.951	-3.538	-6.300	-5.210	-6.242
6.0	6.00	0.060	-3.458	-8.122	-3.273	-5.796	-4.749	-5.687
6.0	6.50	0.050	-3.152	-7.410	-3.030	-5.348	-4.344	-5.203
6.0	7.00	0.042	-2.874	-6.792	-2.805	-4.946	-3.982	-4.775
6.0	7.50	0.036	-2.619	-6.248	-2.595	-4.581	-3.657	-4.392
6.0	8.00	0.032	-2.385	-5.764	-2.399	-4.248	-3.361	-4.047
6.0	8.50	0.028	-2.167	-5.330	-2.213	-3.941	-3.091	-3.734
6.0	9.00	0.025	-1.965	-4.939	-2.037	-3.658	-2.842	-3.446
6.0	9.50	0.022	-1.776	-4.582	-1.869	-3.393	-2.610	-3.182
6.0	10.00	0.020	-1.598	-4.257	-1.709	-3.147	-2.395	-2.936
6.0	15.00	0.009	-0.260	-2.034	-0.385	-1.324	-0.805	-1.174
6.0	20.00	0.005	0.603	-0.756	0.558	-0.186	0.206	-0.093
6.0	25.00	0.003	1.222	0.113	1.247	0.601	0.917	0.662
6.0	30.00	0.002	1.701	0.764	1.772	1.188	1.454	1.234

$log\rho Y_e$	T_9	E_f	^{54}Fe		^{55}Fe		^{56}Fe	
			λ_{ec}	λ_{pc}	λ_{ec}	λ_{pc}	λ_{ec}	λ_{pc}
6.5	0.50	0.905	-18.247	-100	-5.715	-52.894	-39.118	-64.298
6.5	1.00	0.880	-11.098	-51.362	-5.650	-28.592	-21.321	-33.464
6.5	1.50	0.837	-8.634	-34.735	-5.549	-20.108	-15.085	-22.939
6.5	2.00	0.777	-7.299	-26.276	-5.354	-15.741	-11.863	-17.541
6.5	2.50	0.701	-6.406	-21.081	-5.063	-13.035	-9.880	-14.211
6.5	3.00	0.612	-5.738	-17.524	-4.746	-11.164	-8.525	-11.923
6.5	3.50	0.517	-5.205	-14.922	-4.447	-9.770	-7.528	-10.238
6.5	4.00	0.424	-4.754	-12.935	-4.168	-8.679	-6.748	-8.940
6.5	4.50	0.343	-4.355	-11.375	-3.903	-7.795	-6.104	-7.911
6.5	5.00	0.277	-3.992	-10.121	-3.647	-7.062	-5.552	-7.076
6.5	5.50	0.226	-3.659	-9.091	-3.403	-6.440	-5.070	-6.382
6.5	6.00	0.187	-3.353	-8.228	-3.170	-5.902	-4.643	-5.793
6.5	6.50	0.157	-3.070	-7.493	-2.949	-5.431	-4.261	-5.285
6.5	7.00	0.134	-2.809	-6.857	-2.741	-5.011	-3.917	-4.840
6.5	7.50	0.115	-2.567	-6.300	-2.544	-4.634	-3.604	-4.445
6.5	8.00	0.100	-2.342	-5.807	-2.357	-4.291	-3.318	-4.090
6.5	8.50	0.088	-2.132	-5.366	-2.179	-3.977	-3.055	-3.769
6.5	9.00	0.078	-1.936	-4.968	-2.008	-3.687	-2.812	-3.476
6.5	9.50	0.069	-1.751	-4.607	-1.845	-3.418	-2.585	-3.207
6.5	10.00	0.062	-1.577	-4.278	-1.688	-3.168	-2.374	-2.958
6.5	15.00	0.027	-0.254	-2.040	-0.379	-1.330	-0.799	-1.180
6.5	20.00	0.015	0.606	-0.759	0.560	-0.189	0.208	-0.096
6.5	25.00	0.010	1.223	0.112	1.248	0.600	0.918	0.660
6.5	30.00	0.007	1.701	0.763	1.773	1.188	1.455	1.234
7.0	0.50	1.217	-17.545	-100	-4.948	-56.042	-35.991	-67.445
7.0	1.00	1.200	-10.390	-52.979	-4.914	-30.209	-19.710	-35.081
7.0	1.50	1.173	-7.918	-35.863	-4.851	-21.236	-13.960	-24.067
7.0	2.00	1.133	-6.596	-27.175	-4.701	-16.640	-10.966	-18.440
7.0	2.50	1.083	-5.734	-21.851	-4.453	-13.805	-9.111	-14.981
7.0	3.00	1.021	-5.104	-18.212	-4.169	-11.851	-7.839	-12.610
7.0	3.50	0.950	-4.613	-15.546	-3.900	-10.394	-6.906	-10.861
7.0	4.00	0.871	-4.213	-13.498	-3.660	-9.241	-6.186	-9.503
7.0	4.50	0.785	-3.874	-11.871	-3.445	-8.290	-5.609	-8.407
7.0	5.00	0.698	-3.578	-10.545	-3.250	-7.486	-5.128	-7.500
7.0	5.50	0.613	-3.312	-9.445	-3.067	-6.794	-4.716	-6.736
7.0	6.00	0.534	-3.067	-8.520	-2.892	-6.194	-4.352	-6.085
7.0	6.50	0.465	-2.836	-7.732	-2.721	-5.669	-4.023	-5.523
7.0	7.00	0.404	-2.618	-7.052	-2.554	-5.206	-3.723	-5.034
7.0	7.50	0.353	-2.410	-6.460	-2.390	-4.794	-3.445	-4.604
7.0	8.00	0.310	-2.212	-5.939	-2.229	-4.423	-3.187	-4.222
7.0	8.50	0.274	-2.024	-5.476	-2.072	-4.087	-2.946	-3.879
7.0	9.00	0.244	-1.845	-5.061	-1.918	-3.780	-2.720	-3.568
7.0	9.50	0.218	-1.674	-4.686	-1.769	-3.497	-2.507	-3.285
7.0	10.00	0.196	-1.511	-4.345	-1.622	-3.235	-2.307	-3.025
7.0	15.00	0.085	-0.235	-2.059	-0.360	-1.350	-0.779	-1.200
7.0	20.00	0.047	0.614	-0.767	0.568	-0.197	0.216	-0.104
7.0	25.00	0.030	1.227	0.108	1.252	0.596	0.922	0.656
7.0	30.00	0.021	1.704	0.761	1.775	1.185	1.457	1.231

$log\rho Y_e$	T_9	E_f	^{54}Fe		^{55}Fe		^{56}Fe	
			λ_{ec}	λ_{pc}	λ_{ec}	λ_{pc}	λ_{ec}	λ_{pc}
7.5	0.50	1.705	-14.323	-100	-4.113	-60.957	-31.105	-72.360
7.5	1.00	1.693	-8.917	-55.464	-4.079	-32.694	-17.239	-37.565
7.5	1.50	1.675	-6.771	-37.550	-4.020	-22.923	-12.281	-25.754
7.5	2.00	1.648	-5.596	-28.473	-3.903	-17.937	-9.674	-19.738
7.5	2.50	1.614	-4.834	-22.923	-3.711	-14.877	-8.044	-16.053
7.5	3.00	1.573	-4.284	-19.139	-3.479	-12.778	-6.916	-13.537
7.5	3.50	1.524	-3.858	-16.373	-3.250	-11.220	-6.082	-11.688
7.5	4.00	1.468	-3.511	-14.251	-3.040	-9.994	-5.437	-10.256
7.5	4.50	1.405	-3.219	-12.565	-2.852	-8.985	-4.918	-9.101
7.5	5.00	1.336	-2.966	-11.188	-2.685	-8.129	-4.489	-8.143
7.5	5.50	1.262	-2.743	-10.040	-2.533	-7.388	-4.126	-7.330
7.5	6.00	1.183	-2.542	-9.064	-2.394	-6.738	-3.811	-6.628
7.5	6.50	1.101	-2.359	-8.225	-2.264	-6.162	-3.533	-6.016
7.5	7.00	1.018	-2.189	-7.494	-2.140	-5.648	-3.284	-5.476
7.5	7.50	0.937	-2.029	-6.852	-2.020	-5.185	-3.056	-4.995
7.5	8.00	0.858	-1.877	-6.284	-1.902	-4.768	-2.845	-4.566
7.5	8.50	0.783	-1.730	-5.778	-1.784	-4.389	-2.647	-4.179
7.5	9.00	0.714	-1.588	-5.324	-1.666	-4.043	-2.459	-3.830
7.5	9.50	0.651	-1.450	-4.915	-1.548	-3.726	-2.280	-3.513
7.5	10.00	0.593	-1.316	-4.545	-1.429	-3.435	-2.109	-3.224
7.5	15.00	0.268	-0.175	-2.121	-0.300	-1.411	-0.719	-1.261
7.5	20.00	0.150	0.639	-0.793	0.594	-0.223	0.242	-0.129
7.5	25.00	0.095	1.240	0.094	1.265	0.583	0.935	0.643
7.5	30.00	0.066	1.711	0.753	1.783	1.178	1.465	1.224
8.0	0.50	2.444	-6.992	-100	-2.981	-68.412	-23.772	-79.815
8.0	1.00	2.437	-5.267	-59.210	-2.958	-36.440	-13.544	-41.311
8.0	1.50	2.424	-4.437	-40.067	-2.923	-25.440	-9.795	-28.271
8.0	2.00	2.406	-3.881	-30.382	-2.857	-19.847	-7.788	-21.647
8.0	2.50	2.383	-3.456	-24.472	-2.746	-16.426	-6.512	-17.602
8.0	3.00	2.355	-3.112	-20.452	-2.600	-14.091	-5.617	-14.850
8.0	3.50	2.322	-2.826	-17.521	-2.440	-12.369	-4.947	-12.836
8.0	4.00	2.283	-2.580	-15.278	-2.283	-11.021	-4.421	-11.283
8.0	4.50	2.240	-2.364	-13.500	-2.135	-9.920	-3.994	-10.036
8.0	5.00	2.192	-2.171	-12.051	-2.000	-8.991	-3.637	-9.006
8.0	5.50	2.139	-1.998	-10.843	-1.875	-8.192	-3.333	-8.133
8.0	6.00	2.081	-1.839	-9.819	-1.760	-7.492	-3.067	-7.383
8.0	6.50	2.019	-1.693	-8.936	-1.652	-6.873	-2.833	-6.727
8.0	7.00	1.952	-1.557	-8.166	-1.550	-6.320	-2.622	-6.147
8.0	7.50	1.882	-1.429	-7.487	-1.454	-5.820	-2.431	-5.630
8.0	8.00	1.808	-1.309	-6.882	-1.360	-5.366	-2.256	-5.164
8.0	8.50	1.732	-1.195	-6.340	-1.269	-4.951	-2.094	-4.741
8.0	9.00	1.653	-1.086	-5.850	-1.180	-4.569	-1.942	-4.355
8.0	9.50	1.574	-0.982	-5.405	-1.091	-4.216	-1.799	-4.002
8.0	10.00	1.493	-0.881	-4.999	-1.004	-3.888	-1.664	-3.676
8.0	15.00	0.817	0.004	-2.305	-0.121	-1.595	-0.537	-1.444
8.0	20.00	0.470	0.718	-0.873	0.672	-0.303	0.321	-0.209
8.0	25.00	0.301	1.281	0.053	1.305	0.542	0.976	0.602
8.0	30.00	0.209	1.735	0.729	1.806	1.154	1.489	1.200

$log\rho Y_e$	T_9	E_f	^{54}Fe		^{55}Fe		^{56}Fe	
			λ_{ec}	λ_{pc}	λ_{ec}	λ_{pc}	λ_{ec}	λ_{pc}
8.5	0.50	3.547	-1.868	-100	-1.621	-79.532	-12.981	-90.935
8.5	1.00	3.542	-1.834	-64.782	-1.610	-42.012	-8.044	-46.883
8.5	1.50	3.534	-1.781	-43.796	-1.599	-29.169	-6.114	-32.000
8.5	2.00	3.521	-1.713	-33.193	-1.580	-22.658	-5.020	-24.458
8.5	2.50	3.506	-1.631	-26.735	-1.545	-18.690	-4.291	-19.866
8.5	3.00	3.487	-1.540	-22.353	-1.490	-15.993	-3.757	-16.752
8.5	3.50	3.464	-1.442	-19.166	-1.419	-14.014	-3.341	-14.481
8.5	4.00	3.438	-1.340	-16.733	-1.338	-12.476	-3.004	-12.737
8.5	4.50	3.408	-1.237	-14.808	-1.252	-11.228	-2.721	-11.344
8.5	5.00	3.375	-1.135	-13.244	-1.165	-10.184	-2.479	-10.198
8.5	5.50	3.339	-1.035	-11.943	-1.079	-9.291	-2.266	-9.233
8.5	6.00	3.299	-0.937	-10.842	-0.996	-8.516	-2.076	-8.406
8.5	6.50	3.256	-0.841	-9.896	-0.915	-7.833	-1.905	-7.686
8.5	7.00	3.209	-0.748	-9.071	-0.837	-7.225	-1.748	-7.052
8.5	7.50	3.159	-0.658	-8.345	-0.760	-6.679	-1.603	-6.488
8.5	8.00	3.106	-0.571	-7.700	-0.685	-6.184	-1.468	-5.981
8.5	8.50	3.050	-0.485	-7.121	-0.611	-5.732	-1.341	-5.522
8.5	9.00	2.990	-0.403	-6.598	-0.538	-5.317	-1.222	-5.104
8.5	9.50	2.928	-0.323	-6.123	-0.466	-4.934	-1.108	-4.720
8.5	10.00	2.863	-0.245	-5.688	-0.394	-4.578	-0.999	-4.366
8.5	15.00	2.109	0.418	-2.738	0.290	-2.028	-0.116	-1.877
8.5	20.00	1.402	0.945	-1.108	0.900	-0.537	0.551	-0.443
8.5	25.00	0.936	1.406	-0.074	1.430	0.415	1.102	0.475
8.5	30.00	0.656	1.808	0.654	1.879	1.079	1.563	1.125
9.0	0.50	5.179	-0.148	-100	-0.330	-95.981	-1.756	-100
9.0	1.00	5.176	-0.141	-73.015	-0.329	-50.245	-1.716	-55.116
9.0	1.50	5.170	-0.129	-49.294	-0.333	-34.667	-1.653	-37.498
9.0	2.00	5.162	-0.113	-37.326	-0.338	-26.791	-1.569	-28.591
9.0	2.50	5.151	-0.092	-30.052	-0.337	-22.007	-1.470	-23.182
9.0	3.00	5.138	-0.067	-25.127	-0.325	-18.767	-1.365	-19.526
9.0	3.50	5.122	-0.038	-21.554	-0.304	-16.402	-1.260	-16.870
9.0	4.00	5.105	-0.006	-18.833	-0.272	-14.576	-1.157	-14.837
9.0	4.50	5.085	0.030	-16.686	-0.234	-13.105	-1.058	-13.222
9.0	5.00	5.062	0.068	-14.944	-0.190	-11.884	-0.962	-11.898
9.0	5.50	5.037	0.109	-13.499	-0.142	-10.848	-0.870	-10.789
9.0	6.00	5.010	0.152	-12.279	-0.092	-9.953	-0.781	-9.843
9.0	6.50	4.980	0.197	-11.233	-0.041	-9.170	-0.695	-9.024
9.0	7.00	4.948	0.244	-10.324	0.012	-8.477	-0.611	-8.305
9.0	7.50	4.914	0.292	-9.525	0.066	-7.858	-0.529	-7.667
9.0	8.00	4.878	0.342	-8.816	0.121	-7.300	-0.450	-7.097
9.0	8.50	4.839	0.392	-8.182	0.176	-6.793	-0.371	-6.583
9.0	9.00	4.797	0.444	-7.610	0.232	-6.329	-0.294	-6.116
9.0	9.50	4.754	0.495	-7.092	0.288	-5.902	-0.219	-5.688
9.0	10.00	4.708	0.547	-6.618	0.345	-5.508	-0.144	-5.296
9.0	15.00	4.131	1.037	-3.418	0.902	-2.707	0.524	-2.556
9.0	20.00	3.390	1.419	-1.608	1.371	-1.037	1.034	-0.943
9.0	25.00	2.621	1.733	-0.413	1.755	0.077	1.433	0.137
9.0	30.00	1.973	2.023	0.434	2.093	0.860	1.779	0.905

$log\rho Y_e$	T_9	E_f	^{54}Fe		^{55}Fe		^{56}Fe	
			λ_{ec}	λ_{pc}	λ_{ec}	λ_{pc}	λ_{ec}	λ_{pc}
9.5	0.50	7.583	1.215	-100	0.821	-100	0.425	-100
9.5	1.00	7.581	1.217	-85.136	0.821	-62.366	0.429	-67.238
9.5	1.50	7.577	1.221	-57.381	0.817	-42.754	0.436	-45.585
9.5	2.00	7.571	1.226	-43.398	0.811	-32.863	0.447	-34.663
9.5	2.50	7.564	1.232	-34.917	0.810	-26.871	0.461	-28.047
9.5	3.00	7.555	1.240	-29.188	0.815	-22.827	0.479	-23.587
9.5	3.50	7.545	1.249	-25.042	0.826	-19.890	0.499	-20.357
9.5	4.00	7.532	1.258	-21.892	0.843	-17.635	0.521	-17.896
9.5	4.50	7.519	1.269	-19.412	0.865	-15.832	0.545	-15.948
9.5	5.00	7.503	1.281	-17.405	0.890	-14.345	0.571	-14.359
9.5	5.50	7.486	1.295	-15.744	0.918	-13.092	0.598	-13.034
9.5	6.00	7.468	1.310	-14.344	0.948	-12.017	0.627	-11.908
9.5	6.50	7.448	1.326	-13.146	0.980	-11.083	0.657	-10.937
9.5	7.00	7.426	1.344	-12.107	1.014	-10.261	0.688	-10.088
9.5	7.50	7.403	1.364	-11.197	1.049	-9.530	0.721	-9.340
9.5	8.00	7.378	1.385	-10.391	1.085	-8.875	0.755	-8.672
9.5	8.50	7.351	1.408	-9.672	1.123	-8.282	0.791	-8.073
9.5	9.00	7.323	1.433	-9.025	1.161	-7.743	0.828	-7.530
9.5	9.50	7.293	1.458	-8.439	1.200	-7.249	0.866	-7.035
9.5	10.00	7.261	1.486	-7.905	1.240	-6.795	0.905	-6.583
9.5	15.00	6.860	1.793	-4.334	1.655	-3.624	1.332	-3.472
9.5	20.00	6.307	2.070	-2.343	2.021	-1.771	1.711	-1.677
9.5	25.00	5.624	2.292	-1.018	2.312	-0.528	2.006	-0.468
9.5	30.00	4.859	2.481	-0.051	2.548	0.376	2.246	0.422
10.0	0.50	11.118	2.401	-100	2.084	-100	1.947	-100
10.0	1.00	11.116	2.402	-100	2.084	-80.184	1.948	-85.056
10.0	1.50	11.113	2.403	-69.264	2.084	-54.637	1.950	-57.468
10.0	2.00	11.110	2.405	-52.315	2.085	-41.780	1.953	-43.580
10.0	2.50	11.105	2.407	-42.055	2.088	-34.009	1.955	-35.185
10.0	3.00	11.099	2.409	-35.141	2.094	-28.781	1.958	-29.540
10.0	3.50	11.091	2.412	-30.149	2.102	-24.997	1.961	-25.465
10.0	4.00	11.083	2.415	-26.366	2.112	-22.109	1.965	-22.370
10.0	4.50	11.074	2.418	-23.394	2.123	-19.813	1.969	-19.930
10.0	5.00	11.063	2.422	-20.993	2.136	-17.934	1.974	-17.948
10.0	5.50	11.052	2.426	-19.011	2.150	-16.359	1.980	-16.301
10.0	6.00	11.039	2.431	-17.344	2.164	-15.017	1.987	-14.908
10.0	6.50	11.025	2.437	-15.920	2.179	-13.857	1.995	-13.711
10.0	7.00	11.011	2.443	-14.688	2.196	-12.842	2.003	-12.669
10.0	7.50	10.995	2.450	-13.611	2.212	-11.944	2.013	-11.753
10.0	8.00	10.978	2.458	-12.659	2.230	-11.143	2.024	-10.940
10.0	8.50	10.959	2.467	-11.811	2.249	-10.422	2.037	-10.212
10.0	9.00	10.940	2.477	-11.050	2.268	-9.769	2.050	-9.556
10.0	9.50	10.920	2.488	-10.363	2.289	-9.174	2.065	-8.960
10.0	10.00	10.898	2.500	-9.738	2.310	-8.628	2.081	-8.416
10.0	15.00	10.624	2.663	-5.599	2.554	-4.889	2.300	-4.737
10.0	20.00	10.241	2.839	-3.334	2.800	-2.762	2.539	-2.669
10.0	25.00	9.751	2.990	-1.850	3.008	-1.360	2.740	-1.300
10.0	30.00	9.163	3.119	-0.773	3.180	-0.346	2.906	-0.301

$log\rho Y_e$	T_9	E_f	^{54}Fe		^{55}Fe		^{56}Fe	
			λ_{ec}	λ_{pc}	λ_{ec}	λ_{pc}	λ_{ec}	λ_{pc}
10.5	0.50	16.310	3.458	-100	3.313	-100	3.210	-100
10.5	1.00	16.309	3.458	-100	3.314	-100	3.210	-100
10.5	1.50	16.307	3.459	-86.714	3.314	-72.087	3.211	-74.918
10.5	2.00	16.304	3.459	-65.406	3.314	-54.870	3.211	-56.671
10.5	2.50	16.301	3.460	-52.530	3.315	-44.485	3.211	-45.661
10.5	3.00	16.297	3.461	-43.874	3.317	-37.514	3.211	-38.273
10.5	3.50	16.292	3.462	-37.638	3.320	-32.486	3.210	-32.954
10.5	4.00	16.286	3.463	-32.922	3.324	-28.665	3.210	-28.926
10.5	4.50	16.280	3.464	-29.225	3.328	-25.644	3.209	-25.760
10.5	5.00	16.273	3.465	-26.244	3.333	-23.185	3.210	-23.199
10.5	5.50	16.265	3.467	-23.788	3.338	-21.136	3.210	-21.078
10.5	6.00	16.256	3.468	-21.726	3.343	-19.400	3.211	-19.290
10.5	6.50	16.247	3.471	-19.969	3.349	-17.906	3.212	-17.759
10.5	7.00	16.237	3.473	-18.451	3.355	-16.605	3.214	-16.432
10.5	7.50	16.226	3.476	-17.126	3.362	-15.460	3.217	-15.269
10.5	8.00	16.214	3.479	-15.958	3.369	-14.442	3.220	-14.239
10.5	8.50	16.202	3.483	-14.920	3.377	-13.531	3.224	-13.321
10.5	9.00	16.189	3.487	-13.990	3.386	-12.708	3.229	-12.495
10.5	9.50	16.175	3.492	-13.151	3.395	-11.962	3.234	-11.748
10.5	10.00	16.160	3.498	-12.390	3.405	-11.280	3.241	-11.068
10.5	15.00	15.973	3.581	-7.396	3.533	-6.686	3.342	-6.534
10.5	20.00	15.711	3.683	-4.713	3.675	-4.141	3.470	-4.047
10.5	25.00	15.375	3.775	-2.984	3.804	-2.493	3.586	-2.433
10.5	30.00	14.965	3.857	-1.748	3.916	-1.321	3.686	-1.275
11.0	0.50	23.934	4.408	-100	4.355	-100	4.255	-100
11.0	1.00	23.933	4.408	-100	4.355	-100	4.255	-100
11.0	1.50	23.932	4.409	-100	4.355	-97.706	4.255	-100
11.0	2.00	23.930	4.409	-84.622	4.355	-74.087	4.255	-75.887
11.0	2.50	23.928	4.409	-67.906	4.355	-59.860	4.256	-61.036
11.0	3.00	23.925	4.409	-56.689	4.356	-50.329	4.256	-51.088
11.0	3.50	23.922	4.410	-48.624	4.357	-43.472	4.256	-43.940
11.0	4.00	23.918	4.411	-42.537	4.358	-38.280	4.257	-38.542
11.0	4.50	23.913	4.411	-37.774	4.360	-34.194	4.257	-34.310
11.0	5.00	23.908	4.412	-33.941	4.362	-30.881	4.258	-30.895
11.0	5.50	23.903	4.413	-30.787	4.364	-28.136	4.259	-28.077
11.0	6.00	23.897	4.414	-28.144	4.367	-25.818	4.260	-25.708
11.0	6.50	23.891	4.416	-25.896	4.369	-23.833	4.261	-23.686
11.0	7.00	23.884	4.417	-23.957	4.372	-22.111	4.262	-21.938
11.0	7.50	23.877	4.419	-22.267	4.376	-20.601	4.264	-20.410
11.0	8.00	23.869	4.421	-20.780	4.380	-19.264	4.266	-19.062
11.0	8.50	23.860	4.423	-19.461	4.384	-18.071	4.269	-17.862
11.0	9.00	23.851	4.426	-18.280	4.389	-16.999	4.272	-16.786
11.0	9.50	23.842	4.429	-17.218	4.395	-16.029	4.275	-15.815
11.0	10.00	23.832	4.432	-16.257	4.401	-15.146	4.278	-14.934
11.0	15.00	23.704	4.481	-9.994	4.481	-9.284	4.335	-9.132
11.0	20.00	23.526	4.543	-6.682	4.568	-6.110	4.406	-6.016
11.0	25.00	23.296	4.599	-4.581	4.645	-4.090	4.471	-4.030
11.0	30.00	23.016	4.648	-3.101	4.712	-2.673	4.527	-2.628

Tab. II: Comparison of electron capture rates on ^{54,56}Fe using this model (QRPA), TQRPA [29] and LSSM [20] at selected temperature and density scales.

	$log\rho Y_e$	T_9	λ_{ec}^{QRPA}	λ_{ec}^{TQRPA}	λ_{ec}^{LSSM}
^{54}Fe					
	7	1	4.07E-11	2.11E-13	1.33E-11
	7	1.5	1.21E-08	4.16E-08	3.48E-09
	7	2	2.54E-07	1.04E-06	7.78E-08
	7	3	7.87E-06	2.44E-05	3.30E-06
	7	5	2.64E-04	5.52E-04	1.90E-04
	7	10	3.08E-02	6.27E-02	3.10E-02
	8	1	5.41E-06	3.84E-12	3.30E-06
	8	1.5	3.66E-05	7.26E-07	1.04E-05
	8	2	1.32E-04	1.79E-05	3.87E-05
	8	3	7.73E-04	4.06E-04	3.41E-04
	8	5	6.75E-03	8.11E-03	5.00E-03
	8	10	1.32E-01	2.63E-01	1.33E-01
	9	1	7.23E-01	2.42E-01	6.03E-01
	9	1.5	7.43E-01	2.65E-01	6.27E-01
	9	2	7.71E-01	2.98E-01	6.61E-01
	9	3	8.57E-01	4.09E-01	7.69E-01
	9	5	1.17E+00	1.00E+00	1.18E+00
	9	10	3.52E+00	6.97E+00	3.86E+00
	10	1	2.52E+02	2.99E+02	2.94E+02
	10	1.5	2.53E+02	3.00E+02	2.94E+02
	10	2	2.54E+02	3.01E+02	2.96E+02
	10	3	2.56E+02	3.05E+02	2.99E+02
	10	5	2.64E+02	3.33E+02	3.14E+02
	10	10	3.16E+02	5.13E+02	3.80E+02
^{56}Fe					
	7	1	1.95E-20	1.94E-27	1.92E-20
	7	1.5	1.10E-14	6.52E-10	1.00E-14
	7	2	1.08E-11	2.83E-08	9.51E-12
	7	3	1.45E-08	1.45E-06	1.24E-08
	7	5	7.45E-06	7.11E-05	6.56E-06
	7	10	4.93E-03	1.36E-02	4.85E-03
	8	1	2.86E-14	3.38E-21	2.39E-14
	8	1.5	1.60E-10	4.78E-08	1.24E-10
	8	2	1.63E-08	1.60E-06	1.21E-08
	8	3	2.42E-06	5.09E-05	1.77E-06
	8	5	2.31E-04	1.30E-03	1.87E-04
	8	10	2.17E-02	5.77E-02	2.11E-02
	9	1	1.92E-02	2.30E-07	8.77E-03
	9	1.5	2.22E-02	1.46E-05	1.01E-02
	9	2	2.70E-02	2.09E-04	1.28E-02
	9	3	4.32E-02	4.29E-03	2.40E-02
	9	5	1.09E-01	7.46E-02	8.05E-02
	9	10	7.18E-01	1.75E+00	6.95E-01
	10	1	8.87E+01	8.91E+01	8.67E+01
	10	1.5	8.91E+01	8.95E+01	8.71E+01
	10	2	8.97E+01	9.02E+01	8.83E+01
	10	3	9.08E+01	9.27E+01	9.25E+01
	10	5	9.42E+01	1.07E+02	1.04E+02
	10	10	1.21E+02	2.24E+02	1.34E+02

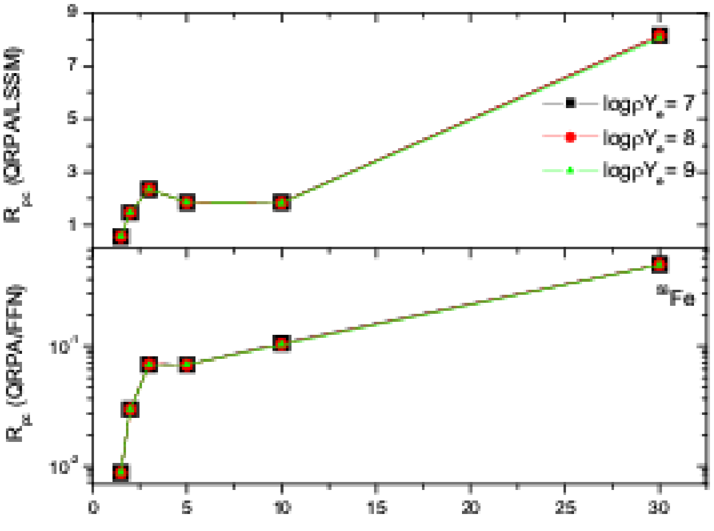

R_{pc} (QRPA/LSSM)
9
7
5
3
1
$\log\rho Y_e = 7$
$\log\rho Y_e = 8$
$\log\rho Y_e = 9$
R_{pc} (QRPA/FFN)
Fe
10^{-1}
10^{-2}
0
5
10
15
20
25
30
T_9